Influence of land cover data on regional forest leaf area index inversion

LI Xianfeng[1], JU Weimin[1], CHEN Shu[1], ZHOU Yanlian[2]

1. *International Institute for Earth System Sciences, Jiangsu Nanjing University, Jiangsu Nanjing* 210093, *China*;
2. *School of Geographic and Oceanographic Sciences, Jiangsu Nanjing University, Jiangsu Nanjing* 210093, *China*

Abstract: In this study, six different land cover datasets were employed in conjunction with MODIS 1km reflectance data to inverse LAI of forests using an algorithm based on the 4-scale geometrical optical model in Jian City, Jiangxi Province, China. Land cover datasets used in this study include five global land cover datasets (Three were produced by the United States Geological Survey (USGS), University of Maryland (UMD), and Boston University (BU), respectively. Two were constructed in Europe.) and a regional land cover map produced using Landsat TM images. For assessing the impact of land cover on the inversion of LAI, LAI images inversely produced with different land cover datasets were compared with LAI data sampled from a 30 m LAI map at 1 km and 4 km scales, respectively. The 30 m LAI map was produced with TM reflectance images and ground measurements of LAI. The results show that the land cover datasets of TM and GLOBCOVER which was created by European Space Agency are the best for the inversion of LAI in this study area. At 1 km scale, the R^2 values of LAI inversed using TM and GLOBCOVER land cover datasets with TM LAI estimated using an statistical model are 0.44 and 0.40, respectively. At 4 km scale, these R^2 values increase to 0.57 and 0.54. The MODIS land cover data of BU is the third best data for the inversion of LAI, the R^2 values between LAI inversed using this land cover dataset and TM LAI are 0.38 and 0.51 at 1 km and 4 km scales, respectively. The land cover datasets of UMD and European GLC2000 resulted in large discrepancies between inversed LAI and TM LAI. The averages of LAI inversed using these two land cover datasets are about 20% lower than TM LAI at 1 km and 4 km scales. Sensitivity analysis shows that inversed LAI is sensitive to clumping index. This study proved that reliable land cover data is required for improving the accuracy of inversed LAI at regional/global scales.

Key words: leaf area index, land cover data, 4-scale model, accuracy of inversion

CLC number: TP79 **Document code:** A

Citation format: Li X F, Ju W M, Chen S and Zhou Y L. 2010. Influence of land cover data on regional forest leaf area index inversion. *Journal of Remote Sensing.* **14**(5): 974—989

1 INTRODUCTION

Land cover plays important roles in physical, chemical, and energy processes of land surface. Therefore, it is a key parameter for global change research (Sellers *et al.*, 1997). In recent years, with the development of remote sensing technology, and the increasing demands for land cover data in global change research and resource management, many countries and international organizations have been conducting studies on regional/global land cover mapping using remote sensing data. For example, five different global land cover datasets were produced by the United States Geological Survey (USGS) and University of Maryland (UMD) using AVHRR data (LoveLand *et al.*, 2000; Hansen *et al.*, 2000), Boston University (BU) using MODIS data (Friedl *et al.*, 2002), the European Joint Research Center of Space Research Institute using VEGETATION data (Bartholomsé *et al.*, 2005) and the European Space Agency using ENVISAT/MERIS data (Defourny *et al.*, 2005). These datasets support the global change research and the extraction of surface parameters (such as LAI, albedo, etc.) from remote sensing data. However, these global land cover datasets exhibit certain inconsistencies, especially in some regions with high complexity of land cover, mainly owing to the differences in classification systems and methods, and data used to produce these datasets (Quaife *et al.*, 2008; Herold *et al.*, 2008). The uncertainties in land cover might induce errors in the parameters derived from remote sensing data.

Leaf area index (LAI) is an extremely important vegetation structural parameter of terrestrial ecosystems (Chen & Cihlar, 1996). At present, the methods used to retrieve LAI from remote sensing data can be broadly classified to two different groups (Fang & Zhang, 2003). The first one is based on the empirical relationship between vegetation index (VI) and LAI. The second type of methods retrieves LAI through inversing radiation transfer or geometric optical models. Although the first type of methods has the advantages of easy implementation and requirement of fewer input parameters, it is not applicable for retrieving LAI at large regional or global scales due to

Received: 2009-11-26; **Accepted**: 2010-04-03
Foundation: 863 Project (No. 2009AA12Z134) and Nation Science Foundation of China (No. 40775061/D0507).
First author biography: LI Xianfeng (1984—), male, master, research in remote sensing in vegetation. E-mail: lixianfeng223@163.com

the considerable spatial and temporal variations in the relationship between VI and LAI. With the inversion techniques, the inversion methods retrieve LAI through adjusting the vegetation structural parameters (including LAI) to minimize the difference between remotely sensed reflectance at various spectral bands and that simulated by radiation transfer or geometric optical models, which were constructed on the basis of the theory of radiation transferring within canopy. This type of methods is suitable for large regional or global applications due to its robust basis of physics. So, it is increasingly used in recent years. For example, the MODIS LAI products were produced mainly using an inversion method. Deng *et al.* (2006) developed a new LAI retrieval algorithm based on the 4-scale geometrical optical model. The unique characteristic of this method is considering the influence of the angles among sun, sensor and target on reflectance and the relationship between LAI and VI in retrieving LAI. This algorithm has proved to be superior to the MODIS LAI algorithm in studies conducted in Canada, Northeast China and red soil hilly region of Jiangxi province of China (Pisek *et al.*, 2007; Liu *et al.*, 2007; Li *et al.*, 2009). Now, this algorithm has been adopted by European Spatial Agency for generating GLOBCARBON LAI products (Garrigues *et al.*, 2008).

Different types of vegetations possess different structures and leaf shapes. Land cover is an essential parameter input into LAI inversion models. The quality of land cover data has a significant impact on inversed LAI (Liu *et al.*, 2008). However, the dependence of inversed LAI on land cover data at regional scales still needs further study. In this study, five global land cover datasets and a regional land cover map produced using Landsat TM images were employed in conjunction with 8d MODIS 1 km reflectance data to inverse LAI of forests using an algorithm based on the 4-scale geometrical optical model (Deng *et al.*, 2006) for Jian City, Jiangxi Province, China. LAI inversed with different land cover datasets were compared with TM LAI, which was produced using TM reflectance images and an empirical model set up according to the ground measurements of LAI, to assess the influence of land cover data on the inversion of LAI quantitatively.

2 STUDY AREA

Jian city (25°58'—27°57' N, 113°46'—115°56' E) is located at the mid-west of Jiangxi province and in the middle reach of Ganjiang River. The total area of this city is 25271 km^2. Mountains and hills account for about 74% of its landmass. It is surrounded by mountains in the east, south and west. The topography declines from the south to the north and from the west and east edges to the interior. Red soils predominantly distributed. The climate is semitropical monsoon, with an annual mean temperature of 18.6℃ and annual precipitation of 1668 mm. This city is abundant of forest resources. The forest coverage is currently about 65.5%, consisting mainly of the natural secondary forests, which are predominantly coniferous Majorities of conifer forests are Masson Pine, Slash Pine, and Chinese Fir. In addition, broadleaf forests (camphor, quercus,and Muhe) and mixed forests also account for certain proportions of this area.

3 STUDY METHOD

3.1 Model description

LAI was inversed using the algorithm developed by Deng *et al.* (2006). This algorithm is based on the 4-scale geometrical optical model, which was employed to construct the look-up tables representing the relationship of LAI with simple ratio (SR) and reduced simple ratio (RSR) under different conditions of land cover types and sensor-sun-target angle combination. SR and RSR are calculated as:

$$\mathrm{SR} = \rho_{\mathrm{nir}} / \rho_{\mathrm{red}} \tag{1}$$

$$\mathrm{RSR} = \mathrm{SR} \times (\rho_{\mathrm{SWIRmax}} - \rho_{\mathrm{SWIR}}) / (\rho_{\mathrm{SWIRmax}} - \rho_{\mathrm{SWIRmin}}) \tag{2}$$

where, ρ_{red}, ρ_{nir} and ρ_{SWIR} are the reflectance in red, near infrared (NIR) and short-wave infrared (SWIR) bands, respectively; ρ_{SWIRmax} and ρ_{SWIRmin} are the maximum and minimum values of ρ_{SWIR}, respectively. They are related to land cover types.

Considering the dependence of the relationship between LAI and SR/RSR on variations in solar zenith angle, view zenith angle and the relative azimuth angle between the sun and sensor, the effective leaf area index (L_{E}) can be expressed as:

$$L_{\mathrm{E}} = f_{\mathrm{LE\_SR}}\left(\mathrm{SR} \times f_{\mathrm{BRDF}}(\theta_{\mathrm{v}}, \theta_{\mathrm{s}}, \phi)\right) \tag{3}$$

$$L_{\mathrm{E}} = f_{\mathrm{LE\_RSR}}\left(\mathrm{SR} \times \left(\frac{\rho_{\mathrm{SWIRmax}} - \rho_{\mathrm{SWIR}} f_{\mathrm{SWIR-BRDF}}(\theta_{\mathrm{v}}, \theta_{\mathrm{s}}, \phi)}{\rho_{\mathrm{SWIRmax}} - \rho_{\mathrm{SWIRmin}}}\right) \times f_{\mathrm{BRDF}}(\theta_{\mathrm{v}}, \theta_{\mathrm{s}}, \phi)\right) \tag{4}$$

where, $f_{\mathrm{LE\_SR}}$ and $f_{\mathrm{LE\_RSR}}$ are the functions describing the relationships of L_{E} with SR and RSR at a specific sun, sensor and target angle combination and they are simulated by the 4-scale geometrical optical model, both depending on land cover types; f_{BRDF} and $f_{\mathrm{SWIR\_B\ RDF}}$ are the functions quantifying the BRDF effects, depending on the angular reflectance behavior of the spectral bands involved, which are described mathematically based on the modified Roujean's model; θ_{v} is the view zenith angle of a sensor; θ_{s} is the solar zenith angle; ϕ is the relative azimuth angle between the sun and sensor.

In Eq. (4), $\mathrm{SR} \times \left(\frac{\rho_{\mathrm{SWIR\ max}} - \rho_{\mathrm{SWIR}} f_{\mathrm{SWIR-BRDF}}(\theta_{\mathrm{v}}, \theta_{\mathrm{s}}, \phi)}{\rho_{\mathrm{SWIR\ max}} - \rho_{\mathrm{SWIR\ min}}}\right) \times f_{\mathrm{BRDF}}(\theta_{\mathrm{v}}, \theta_{\mathrm{s}}, \phi)$ is the RSR with the consideration of the BRDF effects. The relationship of RSR with the LAI is stable and less sensitive to changes in land cover types (Brown *et al.*, 2000). So, only Eq. (4) was used to inverse L_{E} in this study. The details of this inversion algorithm were described in Deng *et al.* (2006). The true LAI is defined as

$$\mathrm{LAI} = L_{\mathrm{E}} / \Omega \tag{5}$$

where, Ω is the clumping index and changes with land cover types, seasons and solar zenith angle. Due to the lack of the

spatially distributed clumping index data, this parameter was assigned for each vegetation type (Table 1) (Tang *et al.*, 2007).

Table 1 Clumping index for typical vegetation types

Vegetation type	Clumping index
Evergreen broadleaf forest	0.63
Deciduous broadleaf forest	0.70
Evergreen needleleaf forest	0.62
Deciduous needleleaf forest	0.68
Mixed forest	0.69
Closed shrublands	0.71
Open shrublands	0.71
Woody savannas	0.72
Savannas	0.70
Grasslands	0.74
Croplands	0.73

3.2 Data used

The reflectance in red, near infrared, and shortwave infrared bands, the view zenith angle, the solar zenith angle, the relative azimuth angle between the sun and sensor were download from the MODIS 09A1 product archive. Five freely available land cover datasets were also downloaded. The 30 m LAI map used for validating inversed LAI was produced with TM reflectance images and ground measurements of LAI.

3.2.1 Ground measurements of LAI and the construction of a 30 m TM LAI map

Ground LAI observations were taken using the TRAC (Tracing Radiation and Architecture of Canopies) instrument at 47 representative forest plots during 24 to 27 July 2008. All observations were made under clear sky condition during the period from 9:30 am to 4:30 pm, strictly following the field operational regulation of TRAC. The size of each plot is about 30 m × 30 m, equal to the grid size of the Landsat TM images. The geographic information and altitude of each plot was recorded using a global positioning system (GPS).

Three scenes of Landsat-5 TM acquired on July 26, 2008 (122/41 and 122/42) and May 16, 2008 (121/41), were used in this study. The first scene (122/41) covers the majority of the study area. The geometric corrections of TM images were conducted in the ENVI 4.3 platform. A 30 m map of forest resources of Jiangxi province was used as the reference for collecting ground control points. The overall error of geometric correction for each TM image was limited to one pixel (30 m) and the projection is UTM/WGS84. Atmospheric correction was performed using the 6S model (Vermote *et al.*, 1997) assuming a continental air mass, mid-latitude summer climate, uniform target, and 30 km atmospheric visibility. After atmospheric correction, radiances of each spectral band were converted into reflectance for calculating VIs and land cover classification. Then three images were joined together. The resultant maps were masked with the administrative boundary of Jian city.

Various VIs indices were calculated from the TM reflectance data and the R^2 value of each VI with the measured LAI was also calculated. It was found that NDVI exponentially transformed is the best predictor of LAI in this region (R^2=0.68, RMSE=0.25, N=47) (Li *et al.*, 2009). The empirical equation for predicting LAI from NDVI is $LAI=0.0284e^{7.7357NDVI}$. The average of LAI predicted by this equation is 2.77 while that of measured LAI is 2.88. Therefore, this equation was used to produce a map of forest LAI at 30 m resolution. Then, this 30 m LAI map was resampled to 1 km and 4 km resolutions to act as the benchmark for validating inversed LAI. Fig. 1 shows the spatial distribution of LAI at 30 m resolution. Since there was no any LAI measurement taken at croplands, LAI was only calculated for forested pixels. LAI of forests showed distinguishable spatial distribution patterns. In the eastern and northwestern parts, LAI was in the range from 3 to 5. In the southwest area, LAI was relatively high, generally above 6.

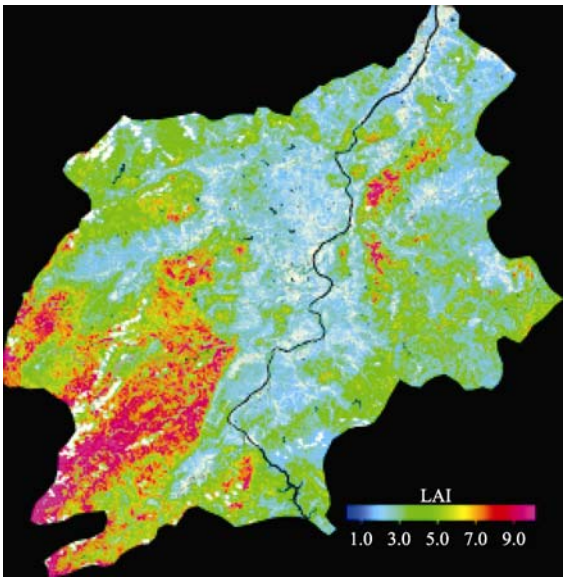

Fig. 1 30 m TM LAI map of Jian city produced using an empirical model

3.2.2 MODIS reflectance data

The 500 m MODIS 8d MOD09A1 product on 28 July 2008 was used in this study. The projection of the MOD09A1 product is Sinusoidal and different from that of other datasets. This product was projected into UTM/WGS 84 and resampled to 1 km resolution. The MOD09A1 product contains reflectance values of bands 1 to 7, quality flags, solar zenith angle, view zenith angle, and the relative azimuth angle between the sun and sensor. Only reflectance in red, near infrared and short infrared bands, quality flags and three angles were required in the LAI inversion model. They were extracted from the MOD09A1 product to generate a new dataset, which was clipped using the administrative boundary of Jian city.

3.2.3 Land cover datasets

Six different land cover datasets were used, including five freely available global land cover datasets and a 30 m map of forest distribution created using Landsat TM images in 1996.

The 30 m map of forest distribution was kindly provided by meteorological bureau of Jiangxi province. This dataset classifies lands into 14 cover types, namely broadleaf forest, needle leaf forest, mixed forest, bamboo, sparse vegetation, shrub land, open forest, barren land, cropland, water body, shadow of hill, urban and built-up, grassland and Island of Poyang Lake. For convenience, this dataset was named as TM land cover data in following sections. The TM land cover map was resampled to 1 km resolution. The dominant cover type was assigned to each resampled 1km×1km pixel. The five global land cover datasets used are:

(1) The global land cover dataset at 1 km resolution produced by the University of Maryland using data from the Advanced Very High Resolution Radiometer (AVHRR) in years 1992 and 1993 and the temporal matrix supervised classification method based on the classification system of the International Geosphere-Biosphere Program (IGBP). There are totally 14 cover types in this dataset. This dataset was named as the UMD land cover dataset.

(2) The global land cover dataset at 1 km resolution produced through the collaboration of the United State Geological Survey (USGS), University of Nebraska-Lincoln (UNL), and the Joint Research Centre of the European Commission using the same data source as the UMD land cover dataset and an unsupervised classification method based on the IGBP classification system. There are 24 land cover types in total in this dataset, which was named as the USGS land cover dataset.

(3) The global land cover dataset at 1 km resolution produced by Boston University (BU) using the MODIS data and the decision tree and artificial neural network classification methods based on the IGBP classification system. 17 land cover types consist of 11 natural vegetation classes, three artificial land classes, ice and snow, permanent barren land or sparse vegetation, and water body. This dataset was named as MODIS land cover dataset.

(4) The global land cover dataset at 1 km resolution was produced by the European Commission's Joint Research Centre using the series of daily reflectance and NDVI from VEGETATION during the period from November 1999 to December 2000 and the bottom-up classification approach based on the land cover classification system (LCCS) of Food and Agriculture Organization (FAO). There are totally 22 land cover types in this dataset, which was named as GLC2000 land cover dataset.

(5) The global land cover dataset at 300m resolution was generated by European Space Agency (ESA) in cooperation with other international organizations using the bimonthly composite ENVISAT/MERIS data during the period from December 2004 to June 2006 and a computer automation and regionally-tuned classification method based on the LCCS classification system of FAO. There are totally 22 land cover types in this dataset, which was named as GLOBCOVER land cover dataset. This dataset was also resampled into 1km resolution.

These six land cover datasets are different in classification and coding systems. The LAI inversion model used in this study requires the land cover data on the basis of IGBP classification and MODIS land cover coding system. Therefore, conversions were made for USGS, UMD, GLC2000, GLOBCOVER and TM land cover datasets to make them compatible with the IGBP/MODIS classification and coding systems. The conversion relationships of classification codes used by different land cover datasets are shown in Table 2.

Table 2 Conversion relationship of classification codes used in different land cover datasets

IGBP/MODIS	USGS	UMD	GLOBCOVER	GLC2000	TM
1 Evergreen needle leaf forest	14	1	70	4, 10	2, 4, 12
2 Evergreen broad leaf forest	13	2	40, 160, 170	1, 7, 8	1
3 Deciduous needle leaf forest	12	3	90	5	–
4 Deciduous broad leaf forest	11	4	50, 60	2, 3	–
5 Mixed forest	15	5	100, 110, 120	6, 9	3
6 Dense shrub	8	8	130	11, 12	6
7 Sparse shrub	9	9	150	14	–
8 Woody savannas	21	6	–	–	5
9 Savannas	10, 20, 22	7	–	–	7
10 Grasslands	7	10	140	13	8
11 Permanent wetlands	17, 18	–	180	15	14
12 Croplands	2, 3, 4	11	11, 14	16	10
13 Urban and built-up areas	1	13	190	22	13
14 Cropland/natural vegetation mosaic	5, 6	–	20, 30	17, 18	–
15 Snow and ice	23, 24	12	220	21	–
16 Barren or sparsely vegetated	19	–	200	19	9
17 Water bodies	16	0	210	20	11

3.3 Evaluation of the impact of land cover data on the accuracy of inversed LAI

The influence of land cover data on the inversion of LAI was evaluated by comparing inversed LAI with TM LAI. There are lots of mixed pixels in this study area. With the assumption that each pixel in the 30 m resolution map is purely covered by one type, the proportions of pixels covered by forests in the 1 km and 4 km resolution maps were calculated. The evaluations of inversed LAI were only conducted for pixels in which the area fractions of forests were above 50%. The criteria used to evaluate the influence of land cover data on LAI inversion include the coefficient of determination (R^2), the Root Mean Square Error (RMSE) and the relative difference of mean value (RE) of inversed LAI.

4 RESULTS AND ANALYSISES

4.1 Consistency of different land cover datasets

The proportions of different land cover types calculated from six land cover datasets differ considerably (Table 3). In the USGS and UMD land cover datasets, the forest coverage is less than 10%. This is in contrast with the reality. The study area is rich in forest resource. The forest coverage is up to 65.5% according to the statistical data. In the MODIS, GLOBCOVER and TM land cover datasets, the forest coverage are all above 50%, which is in good agreement with the actual situation. But the forest types are different among these three land cover datasets. In the GLOBCOVER and TM land cover datasets, needle leaf forests account for large proportions, being 41.77% and 37.64%, respectively. In the MODIS land cover dataset, the largest proportion is mixed forests, amounting to 40.66%. While in the GLC2000 land cover dataset, the coverage of deciduous broadleaf forests is up to 63.97%. There are no savannas in the GLOBCOVER and GLC2000 land cover datasets. But in the USGS and UMD land cover datasets, the proportions of savannas are 41.09% and 48.17%, respectively. GLC2000 land cover dataset has large differences with other land cover datasets in water bodies, cropland and urban/built-up. Croplands occupy a large fraction of the study area. But in the GLC2000 land cover dataset, there are no any croplands. While in other land cover datasets, the proportions of croplands are all above 15%. The study area is located in the mid-latitude subtropical zone. No ice and snow exist here. But in the GLC2000 land cover dataset the proportion of ice and snow is up to 14.23%. The large discrepancies among these land cover datasets may be attributed to the differences in the classification system and methods used to produce them. The difference in time when these datasets were constructed might also result in such discrepancies.

4.2 Distribution of inversed LAI

The 1 km LAI inversed using six land cover datasets in conjunction with MOIDIS reflectance and angular data shows considerable differences (Fig. 2). LAI inversed using the MODIS, GLOBCOVER, and TM land cover datasets exhibits similar spatial distribution patterns, with distinguishable spatial variations. LAI of forests in the western part is larger than that in the eastern part (Fig. 2(d), 2(e) and 2(f)). But the proportion of high LAI values (above 7) inversed using the GLOBCOVER and TM land cover datasets is higher than that of LAI inversed using the MODIS land cover data. The spatial distribution of LAI inversed using the MODIS, GLOBCOVER, and TM land cover datasets mostly mirrors that of the 30 m TM LAI. However, LAI inversed using the MODIS, GLOBCOVER, and TM land cover datasets is larger than the 30 m TM LAI in the

Table 3 Proportion of various land cover types in six land cover datasets

/%

Land cover type	USGS	UMD	GLOBCOVER	GLC2000	MODIS	TM
Evergreen needleleaf forest	4.32	9.04	41.77	0	5.56	37.64
Evergreen broadleaf forest	0	0.24	13.60	0	3.12	1.28
Deciduous needleleaf forest	0	0	0	17.41	0.02	0
Deciduous broadleaf forest	1.79	0.08	0.03	62.97	1.46	0
Mixed forest	0.22	0.18	0.63	0.23	40.66	10.35
Mixed forest	0.18	0.06	9.88	0	0.36	4.27
Open shrublands	0	0.03	0	0.65	0.60	0
Woody savannas	0	17.93	0	0	25.02	0.47
Savannas	41.09	30.24	0	0	0.65	3.77
Grasslands	0.19	25.38	0.03	0	1.97	0.66
Permanent wetlands	0.01	0	0	4.49	1.71	0
Croplands	30.63	15.71	30.31	0	16.43	36.87
Urban and built-up	0.03	0.03	0.21	0	0.20	1.67
Cropland/natural vegetation mosaic	20.52	0	2.49	0	1.89	0
Snow and ice	0	0	0	14.23	0	0
Barren or sparsely vegetated	0	0	0	0	0.03	0.14
Water bodies	1.02	1.09	1.05	0	0.32	2.88

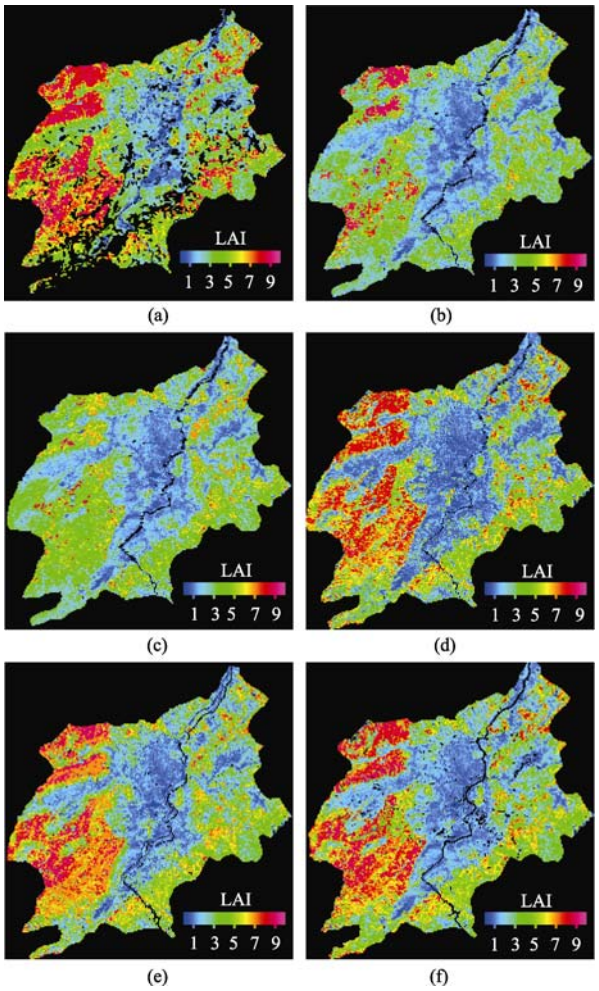

Fig. 2 Maps of LAI at 1 km resolution inversed using the GLC2000 (a), UMD (b), USGS (c), MODIS (d), GLOBCOVER (e) and TM land cover datasets (f) in combination with MODIS reflectance data

northwestern part. The spatial variability of LAI inversed using the UMD and USGS land cover datasets is less obvious (Fig. 2(b) (c)). Inversed LAI are significantly lower than the TM LAI in the western part. The LAI of forests is mostly in the range from 3 to 5. Only a few LAI is larger than 7. Especially, LAI inversed using the USGS land cover dataset is almost totally below 7. As the GLC2000 land cover dataset differ noticeably from other land cover datasets, LAI inversed using this dataset shows very large discrepancy with LAI inversed using other land cover datasets in the eastern part of the study area. In the GLC2000 land cover dataset, parts of forests and croplands were misclassified as snow and ice. In these cases, inversed LAI equals zero (the black area in Fig. 2(a)). Overall, the consistency of LAI inversed using different land cover datasets is better in the middle and east parts than in the west part.

4.3 Effects of land cover data on the accuracy of inversed LAI

Table 4 shows the statistics of LAI inversed using six different land cover datasets compared with resampled TM LAI at 1 km resolution. TM land cover dataset is the best land cover data for LAI inversion among six land cover datasets, with R^2 of inversed LAI equal to 0.44. The GLOBCOVER land cover data is the second best land cover data for LAI inversion (R^2=0.40). The UMD and GLC2000 land cover datasets resulted in large errors in inversed LAI, with R^2 of inversed LAI equal to 0.24 and 0.15, respectively. The maximum and minimum RESE values of inversed LAI are 2.7 and 1.8, resulting from the applications of the GLC2000 and TM land cover datasets to LAI inversion, respectively. The average of LAI inversed using the GLC2000, GLOBACOVER and TM land cover datasets are 3.4%, 5.1% and 2.4% higher compared with that of TM LAI while the averaged LAI inversed using remaining three land cover datasets is lower than averaged TM LAI. The underestimation of LAI inversed using the UMD and USGS land cover datasets are 19.8% and 18.8%, respectively.

In order to limit the influence of errors in remote sensing image registration on assessing the accuracy of inversed LAI, the inversed LAI and TM LAI were compared at 4 km resolution. The agreement between LAI inversed using six different land cover datasets and TM LAI obviously improves. The R^2 of LAI inversed using the TM land cover dataset is the highest (0.57). The R^2 of LAI inversed using the GLC2000 land cover dataset increases to 0.23. However, it is still the lowest one. The

Table 4 Statistics of LAI inversed using six land cover datasets compared with TM LAI

Land cover dataset used in LAI inversion	1 km				4 km			
	R^2	RMSE*	Mean**	RE***	R^2	RMSE*	Mean**	RE***
GLC2000	0.15	2.7	4.2	3.4%	0.23	2.1	4.0	–1.0%
UMD	0.24	2.1	3.2	–19.8%	0.34	1.8	3.1	–21.8%
USGS	0.30	2.0	3.3	–18.8%	0.40	1.6	3.2	–20.5%
MODIS	0.38	1.9	3.9	–4.1%	0.51	1.5	3.8	–5.7%
GLOBCOVER	0.40	1.9	4.3	5.1%	0.54	1.4	4.1	3.1%
TM	0.44	1.8	4.2	2.4%	0.57	1.3	4.0	1.8%

Notes: *RMSE= $\sqrt{1/N\sum_{i=1}^{N}(\mathrm{LAI}_{\mathrm{inv}}(i)-\mathrm{LAI}_{\mathrm{TM}}(i))^2}$, N is the number of the forested pixels; $\mathrm{LAI}_{\mathrm{inv}}$ and $\mathrm{LAI}_{\mathrm{TM}}$ are the inversed LAI and resampled TM LAI, respectively;

**Mean= $\frac{1}{N}\sum_{i=1}^{N}\mathrm{LAI}_{\mathrm{inv}}(i)$, being the average LAI of all forested pixels.

***RE= $(\overline{\mathrm{LAI}_{\mathrm{inv}}}-\overline{\mathrm{LAI}_{\mathrm{TM}}})/\overline{\mathrm{LAI}_{\mathrm{TM}}}\times100\%$, being the relative error of the average inversed LAI, $\overline{\mathrm{LAI}_{\mathrm{inv}}}$ is the average of inversed LAI; $\mathrm{LAI}_{\mathrm{TM}}$ is the average of resampled TM LAI.

accuracy of LAI inversed using the TM, GLOBCOVER and MODIS land cover datasets is still higher than that of LAI inversed using other three land cover datasets at 4 km resolution. All RMSE values of LAI inversed using six different land cover datasets are lower at 4 km resolution than those at 1 km resolution. The lowest RMSE of inversed LAI was 1.3 (using the TM land cover dataset) and the highest RMSE of inversed LAI was 2.1 (using the GLC2000 land cover dataset). The RE values did not change significantly at 4 km resolution compared with those at 1 km resolution.

4.4 Sensitivity analysis of inversed LAI to parameters

Clumping index (Ω), maximum and minimum values of reflectance in shortwave infrared band ($\rho_{SWIRmax}$ and $\rho_{SWIRmin}$) are the key input parameters in the LAI inversion model. In order to evaluate the influence of these parameters on inversed LAI, sensitivity analysis was carried out by increasing or decreasing these parameters by 10%. Table 5 shows the statistics of LAI inversed using different values of Ω, $\rho_{SWIRmax}$ and $\rho_{SWIRmin}$ compared with TM LAI at 4 km resolution. When Ω was increased by 10%, the averages of LAI inversed using six land cover datasets were all lower than the average of TM LAI. When Ω was decreased by 10%, the agreement of LAI inversed using the UMD and USGS land cover datasets with TM LAI increased. As indicated by equation 4, $\rho_{SWIRmax}$ and $\rho_{SWIRmin}$ affect the inversed effective leaf area index (L_E) and further affect inversed LAI. When $\rho_{SWIRmax}$ and $\rho_{SWIRmin}$ were increased, the inversed LAI would increase. On the contrary, when $\rho_{SWIRmax}$ and $\rho_{SWIRmin}$ were decreased, the inversed LAI would decrease. The responses of inversed LAI to $\rho_{SWIRmax}$ and $\rho_{SWIRmin}$ are non-linear. Inversed LAI is more sensitive to Ω than sensitive to $\rho_{SWIRmax}$ and $\rho_{SWIRmin}$.

Table 5 Statistics of 4 km LAI inversed using different Ω, $\rho_{SWIRmax}$ and $\rho_{SWIRmin}$ values compared with TM LAI

Land cover data	1.1Ω			0.9Ω			$1.1\rho_{SWIRmax}$			$0.9\rho_{SWIRmax}$			$1.1\rho_{SWIRmin}$			$0.9\rho_{SWIRmin}$		
	R^2	RMSE	RE	R^2	RMSE	RE	R^2	RMSE	RE	R^2	RMSE	RE	R^2	RMSE	RE	R^2	RMSE	RE
GLC2000	0.23	2.0	−8.3	0.23	2.1	7.2	0.24	2.1	6.4	0.22	2.1	−10.4	0.23	2.0	0.6	0.23	2.0	−2.3
UMD	0.32	1.9	−27.9	0.36	1.6	−14.6	0.34	1.8	−21.1	0.34	1.8	−22.7	0.34	1.7	−21.6	0.34	1.8	−22.0
USGS	0.38	1.8	−26.6	0.42	1.5	−13.1	0.39	1.6	−19.7	0.41	1.6	−21.3	0.40	1.6	−20.3	0.40	1.6	−20.6
MODIS	0.50	1.5	−12.5	0.53	1.4	2.0	0.53	1.4	−1.4	0.49	1.5	−11.0	0.51	1.5	-4.9	0.51	1.5	−6.4
GLOBACOVER	0.54	1.4	−4.1	0.54	1.5	11.5	0.55	1.5	7.1	0.53	1.4	−1.8	0.54	1.4	4.1	0.54	1.4	2.3
TM	0.57	1.4	−0.2	0.57	1.3	4.5	0.59	1.4	6.3	0.54	1.3	−3.6	0.57	1.4	2.9	0.57	1.3	0.9

5 CONCLUSIONS AND DISCUSSION

In this study, six different land cover datasets were employed in conjunction with MODIS reflectance data to inverse LAI. The LAI estimated using TM remote sensing data and LAI measurements was used as the benchmark to assess the impact of land cover data on regional inversed LAI. The following conclusions can be drawn from this study:

(1) There are large differences in the six land cover datasets (MODIS, USGS, GLOBCOVER, UMD, GLC2000, and TM). Such differences were caused by the differences in methods, remote sensing data and classification systems used to construct land cover datasets. The difference of average LAI inversed using different land cover datasets might be above 20%. Therefore, reliable land cover data is required for improving the accuracy of inversed LAI at regional scales.

(2) Among six land cover datasets, the TM land cover dataset is the best for inversing LAI in this study area. The R^2 values of LAI inversed using this land cover dataset are 0.44 at 1 km scale and 0.57 at 4 km scale, repetitively and corresponding RE values are 2.4% and 1.8%. Among the five freely available global land cover datasets, the GOLBCOVER and MODIS land cover datasets resulted in better reliability of inversed LAI and are practically applicable for inversing LAI in this study area. The GLC2000 and UMD land cover datasets might induce noticeable errors in inversed LAI.

(3) Sensitivity analysis showed that clumping index (Ω) has a significant influence on inversed LAI. However, this parameter was assumed to change with land cover type only in this study. Its variations with the development stage of forests and season were ignored. Such simple treatment for this parameter might increase the uncertainties of inversed LAI. The accuracy of inversed LAI will be improved if clumping index can be retrieved from the multi-angle remote sensing data.

In this study, a 30 m TM LAI map constructed using the empirical model based on the ground measurements of LAI data was used as the benchmark to assess the accuracy of the inversed LAI. Doubtlessly, there are some uncertainties in the 30 m TM LAI data, which influence the evaluation of inversed LAI to certain extent. The sensitivity of inversed LAI to land cover data varies for different inversion models. In this study, only the model developed by Deng *et al.* (2006) was used. This is the inadequacies of this study and needs further remedy. Land cover data is an important factor affecting the inversion of LAI. Other factors, such as topographic effect and background reflectance can also affect the inversion of forest LAI. The exclusion of these factors in the inversion of LAI is one of candidates resulting in certain differences between the inversed LAI and TM LAI. Further efforts should be made to use the multi-angle remote sensing data (such as MISR) to retrieve background reflectance and correct on the influences of topography on reflectance data to improve the reliability of LAI inversed using MODIS reflectance data.

REFERENCES

Bartholomé E and Belward S. 2005. GLC2000: a new approach to global land covers mapping from earth observation data. *International Journal of Remote Sensing*, **26**(9): 1959—1977

Brown L, Chen J M, Leblanc S G and Cihlar J. 2000. A shortwave infrared modification to the simple ratio for LAI retrieval in boreal forests: an image and model analysis. *Remote Sensing of Environment*, **71**: 16—25

Chen J M and Cihlar J. 1996. Retrieving leaf area index of boreal conifer forests using Landsat TM images. *Remote Sensing of Environment*, **55**: 153—162

Defourny P, Vancutsem C, Bicheron P, Nino F, Schouten L and Leroy M. 2006. Globcover: a 300 m global land cover product for 2005 using ENVISAT MERIS time series. Proceedings of ISPRS Commission VII Symposium: Remote Sensing from Pixels to Processes. Enschedes, The Netherlands

Deng F, Chen J M, Plummer S, Chen M Z and Pisek J. 2006. Algorithm for global leaf area index retrieval using satellite imagery. *IEEE Transactions on Geoscience and Remote Sensing of Environment*, **44**(8): 2219—2229

Fang X Q and Zhang W C. 2003. The application of remotely sensed data to the estimation of the leaf area index. *Remote Sensing for Land & Resources*, (3): 58—62

Friedl M A, McIver D K, Hodges J C F, Zhang X Y, Muchoney D, Strahler A H, Woodcock C E, Gopal S, Schneider A, Cooper A, Baccini A, Gao F and Schaaf C. 2002. Global land cover mapping from MODIS: algorithms and early results. *Remote Sensing of Environment*, **83**: 287—302

Garrigues S, Lacaze R, Baret F, Morisette J T, Weiss M, Nickeson J E, Fernandes R, Plummer S, Shabanov N V, Myneni R B, Knyazikhin Y and Yang W. 2008. Validation and intercomparison of global Leaf Area Index products derived from remote sensing data. *Journal of Geophysical Research*, **113**, G02028, doi:10.1029/2007JG000635

Hansen M C, DeFries R S, Townshend J R G and Sohlberg R. 2000. Global land cover classification at 1km spatial resolution using a classification tree approach. *International Journal of Remote Sensing*, **21**(6/7): 1331—1364

Herold M, Mayaux P, Woodcock C E, Baccini A and Schmullius C. 2008. Some challenges in global land cover mapping: An assessment of agreement and accuracy in existing 1 km datasets. *Remote Sensing of Environment*, **112**: 2538—2556

Li X F, Ju W M, Zhou Y L and Chen S. 2009. Retrieving leaf area index of forests in red soil hilly region using remote sensing data. Proceedings of the Second International Conference on Earth Observation for Global Changes.

Liu R, Chen J M, Liu J, Deng F and Sun R. 2007. Application of a new leaf area index algorithm to China's landmass using MODIS data for carbon cycle research. *Journal of Environmental Management*, **85**: 649—658

Loveland T R, Reed B C, Brown J F, Ohlen D O, Zhu Z Yang L and Merchant J W. 2000. Developments of a global land cover characteristics database and IGBP DISCover from 1-km AVHRR Data. *International Journal of Remote Sensing*, **21** (6/7): 1303—1330

Pisek J, Chen J M and Deng F. 2007. Assessment of a global leaf area index product from SPOT-4 vegetation data over selected sites in Canada. *Canadian Journal of Remote Sensing*, **33**(4): 341—358

Quaife T, Quegan S, Disney M, Lewis P, Lomass M and Woodward F I. 2008. Impact of land cover uncertainties on estimates of biospheric carbon fluxes. *Global Biogeochemical Cycles*, **22**, GB4016, doi:10.1029/2007GB003097

Sellers P J, Dickinson R E, Randall D A, Betts A K, Hall F G, Berry J A, Collatz G J, Denning A S, Mooney H A, Nobre C A, Sato N, Field C B and Henderson-sellers A. 1997. Modeling the Exchanges of energy, water, and carbon between continents and the atmosphere. *Science*, **275**: 502—509

Tang S, Chen J M, Zhu X, Li X Chen M, Sun R, Zhou Y, Deng F and Xie D. 2007. LAI inversion algorithm based on directional reflectance kernels. *Journal of Environmental Management*, **85**: 638—648

Vermote E F, Tanre D, Deuze' J L, Herman M and Morcrette J J. 1997. Second simulation of the satellite signal in the solar spectrum, 6S: an overview. *IEEE Transactions on Geoscience and Remote Sensing of Environment*, **35**(3): 675—686

地表覆盖分类数据对区域森林叶面积指数反演的影响

李显风[1], 居为民[1], 陈 姝[1], 周艳莲[2]

1. 南京大学 国际地球系统科学研究所, 江苏 南京 210093;
2. 南京大学 地理与海洋科学学院, 江苏 南京 210093

摘 要: 以江西省吉安市为研究区, 将 5 种全球地表覆盖分类数据(包括美国地质调查局(USGS)、马里兰大学(UMD)和波士顿大学(BU)生成的 3 套数据和欧洲生成的 2 套数据)以及由 TM 影像生成的区域地表覆盖分类数据, 分别与 MODIS 1 km 反射率资料结合, 利用基于 4 尺度几何光学模型的 LAI 反演方法生成研究区的 LAI。在 1 km 和 4 km 两种尺度上将反演的 LAI 与 TM 资料生成的 LAI 进行比较, 评价地表覆盖分类数据对 LAI 反演结果的影响。结果表明, TM 和欧洲太空局的 GLOBCOVER 地表覆盖分类数据用于反演 LAI 的结果较好, 在 1 km 尺度上, 反演的 LAI 与统计模型估算的 TM LAI 相关的 R^2 分别为 0.44 和 0.40, 在 4 km 尺度上的 R^2 分别为 0.57 和 0.54; 其次为波士顿大学的 MODIS 地表覆盖分类数据, 据其反演的 LAI 与 TM LAI 相关的 R^2 在 1km 和 4 km 尺度上分别为 0.38 和 0.51; 而马里兰大学的 UMD 和欧洲的 GLC2000 地表覆盖分类数据会导致反演的 LAI 存在较大误差, 据其反演的 LAI 与 TM LAI 之间的一致性较差, 在 1 km 和 4 km 两种尺度上平均偏低 20%左右; LAI 的反演结果对聚集度系数具有强的敏感性。该研究表明, 为了提高区域/全球 LAI 反演精度, 需要有高质量的地表覆盖分类数据。

关键词: 叶面积指数, 地表覆盖, 四尺模型, 反演精度

中图分类号: TP79 文献标志码: A

引用格式: 李显风, 居为民, 陈 姝, 周艳莲. 2010. 地表覆盖分类数据对区域森林叶面积指数反演的影响. 遥感学报, **14**(5): 974—989

Li X F, Ju W M, Chen S and Zhou Y L. 2010. Influence of land cover data on regional forest leaf area index inversion. *Journal of Remote Sensing*. **14**(5): 974—989

1 引 言

地表覆盖类型对地表物理、化学和能量循环过程有着非常重要的影响作用, 是进行全球变化研究的重要参数(Sellers 等, 1997)。近年来, 随着遥感技术的发展, 以及全球变化研究和资源管理等对地表覆盖分类数据(land cover data)需求的增加, 许多国家和国际组织相继开展了区域和全球尺度地表覆盖遥感制图研究。如美国地质调查局(USGS)和马里兰大学(UMD)分别利用 AVHRR 数据(Loveland 等, 2000; Hansen 等, 2000)、波士顿大学(BU)利用 MODIS 数据(Friedl 等, 2002)和欧洲联合研究中心空间研究所利用 VEGETATION 数据(Bartholomé 等, 2005)和欧洲太空局利用 ENVISAT/MERIS 数据(Defourny 等, 2005)生成了 5 套全球地表覆盖数据, 支撑全球变化研究的开展和其他地表参数(如叶面积指数(LAI)、反照率等)的遥感提取。由于在分类方法、数据源和分类系统等方面的差异, 这些全球地表覆盖产品存在着不一致性, 在一些地区的差异较大(Quaife 等, 2008; Herold 等, 2008), 导致遥感提取的其他参数存在不确定性。

LAI 是陆地生态系统中一个十分重要的植被结构参数(Chen & Cihlar, 1996)。目前, 利用遥感资料提取 LAI 的方法分为建立植被指数(VI)与 LAI 之间关系的经验模型和利用辐射传输或几何光学模型进行 LAI 反演两大类(方秀琴 & 张万昌, 2003)。虽然前一类方法具有简单易行的优点, 但是由于 VI 与 LAI 之间关系存在着较大的时空变化, 该类方法不适合在大尺度上应用; 而 LAI 模型反演方法利用模型反演技术, 通过调整 LAI 等植被结构参数使建立在植被冠层辐射传输理论基础上的辐射传输或几何光学模型模拟的不同波段反射率逼近遥感观测数

收稿日期: 2009-11-26; 修订日期: 2010-04-03

基金项目: 863 项目(编号: 2009AA12Z134)和国家自然科学基金(编号: 40775061/D0507)。

第一作者简介: 李显风(1984—), 男, 硕士研究生, 主要从事植被遥感等方面的研究工作。E-mail: lixianfeng223@163.com。

据, 进行 LAI 的反演, 物理意义明确, 适用于在区域尺度上提取 LAI。因此, 该方法近年来得到越来越广泛的应用, 如 MODIS 的 LAI 产品就主要是以反演方法生成的。Deng 等(2006)提出了一种基于 4 尺度几何光学模型的 LAI 反演算法, 其特点是考虑了太阳天顶角-传感器天顶角-太阳与传感器之间相对方位角变化对反射率和 LAI 与 VI 之间关系的影响进行 LAI 的反演。在加拿大、中国东北和中国江西省红壤丘陵地区的应用表明, 这种方法反演的 LAI 数据质量要优于 MODIS 的 LAI 产品(Pisek 等, 2007; Liu 等, 2007; Li 等, 2009)。现在, 该方法已经被欧洲航天局用于生成 Globcarbon LAI 产品(Garrigues 等, 2008)。

由于不同类型的植被在冠层结构及叶片形状等方面存在差异, 所以地表覆盖分类数据是 LAI 反演模型的必要输入参数, 其质量影响 LAI 的反演结果(Liu 等, 2008)。在区域尺度上, 这种影响的程度如何还有待深入研究。本文以江西省吉安市为研究区, 将美国和欧洲生成的 5 套全球地表覆盖分类数据以及由 TM 遥感影像生成的区域地表覆盖分类数据分别与 8d 合成的 MODIS 1km 反射率数据结合, 利用 Deng 等(2006)发展的基于 4 尺度光学模型的 LAI 反演算法, 反演研究区的 LAI, 将其与由 TM 数据和 LAI 观测数据生成的 LAI 进行比较, 定量评价地表覆盖分类数据质量对 LAI 反演结果的影响。

2 研究区

吉安市(25°58′—27°57′N, 113°46′—115°56′E)位于江西省中西部, 赣江中游。全市总面积为 25271km^2, 以山地、丘陵为主, 约占土地总面积的 74%, 境内东、南、西三面环山, 地势由南至北, 由东、西边缘向腹地逐渐倾斜, 土壤主要为红壤类型。吉安属中亚热带季风性气候, 年平均气温 18.6℃, 年均降水量 1668mm。境内森林资源丰富, 森林覆盖率达 65.5%, 以天然次生林为主, 针叶林面积比重较大, 主要树种有马尾松、湿地松、杉木和竹林等。另外, 樟树、栎、木荷等阔叶林和针阔混交林也占一定的比例。

3 研究方法

3.1 模型概述

LAI 的反演采用 Deng 等(2006)提出的基于 4 尺度几何光学模型的 LAI 反演算法进行。该算法利用 4 尺度几何光学模型进行模拟试验, 建立不同地表覆盖类型和太阳天顶角-传感器天顶角-太阳与传感器之间相对方位角条件下, LAI 与比值植被指数(SR)和减小的比值植被指数(RSR)之间关系的查找表, 进行 LAI 的反演。SR 和 RSR 分别计算为:

$$\mathrm{SR} = \rho_{\mathrm{nir}} / \rho_{\mathrm{red}} \tag{1}$$

$$\mathrm{RSR} = \mathrm{SR} \times (\rho_{\mathrm{SWIRmax}} - \rho_{\mathrm{SWIR}}) / (\rho_{\mathrm{SWIR\,max}} - \rho_{\mathrm{SWIR\,min}}) \tag{2}$$

式中, ρ_{nir} 和 ρ_{red} 分别为近红外和可见光波段反射率; ρ_{SWIR}、ρ_{SWIRmax} 和 ρ_{SWIRmin} 分别为短波红外反射率、短波红外反射率的最大和最小值。其中 ρ_{SWIRmax} 和 ρ_{SWIRmin} 与地表覆盖类型有关。

如考虑了太阳天顶角-传感器天顶角-太阳与传感器之间相对方位角变化对 LAI 与 SR 和 RSR 之间关系的影响, 有效叶面积指数(L_{E})可以表示为:

$$L_{\mathrm{E}} = f_{\mathrm{LE\_SR}}(\mathrm{SR} \times f_{\mathrm{BRDF}}(\theta_{\mathrm{v}}, \theta_{\mathrm{s}}, \phi)) \tag{3}$$

$$L_{\mathrm{E}} = f_{\mathrm{LE\_RSR}}\left(\mathrm{SR} \times \left(\frac{\rho_{\mathrm{SWIR\,max}} - \rho_{\mathrm{SWIR}} f_{\mathrm{SWIR\_BRDF}}(\theta_{\mathrm{v}}, \theta_{\mathrm{s}}, \phi)}{\rho_{\mathrm{SWIR\,max}} - \rho_{\mathrm{SWIR\,min}}}\right) \times f_{\mathrm{BRDF}}(\theta_{\mathrm{v}}, \theta_{\mathrm{s}}, \phi)\right) \tag{4}$$

式中, $f_{\mathrm{LE\_SR}}$, $f_{\mathrm{LE\_RSR}}$ 为某一特定的太阳天顶角-传感器天顶角-太阳与传感器之间相对方位角条件下 SR 和 RSR 与 LAI 之间的关系, 由 4 尺度几何光学模型模拟确定, 随地表覆盖类型变化; f_{BRDF} 和 $f_{\mathrm{SWIR\_BRDF}}$ 为二向反射分布函数(BRDF)订正因子, 由改进的核驱动模型计算确定; θ_{s} 是太阳天顶角; θ_{v} 是传感器天顶角; ϕ是太阳和传感器之间的相对方位角。

在方程(4)中, $\mathrm{SR} \times \left(\frac{\rho_{\mathrm{SWIR\,max}} - \rho_{\mathrm{SWIR}} f_{\mathrm{SWIR\_BRDF}}(\theta_{\mathrm{v}}, \theta_{\mathrm{s}}, \phi)}{\rho_{\mathrm{SWIR\,max}} - \rho_{\mathrm{SWIR\,min}}}\right) \times f_{\mathrm{BRDF}}(\theta_{\mathrm{v}}, \theta_{\mathrm{s}}, \phi)$ 为考虑了 BRDF 效应的 RSR。RSR 植被指数具有与 LAI 之间关系稳定、受地表覆盖类型影响小的优点(Brown 等, 2000), 所以, 本研究选用公式(4)进行 L_{E} 的反演, 详细的反演步骤可参见文献 Deng 等(2006)。真实 LAI 由下式计算:

$$\mathrm{LAI} = L_{\mathrm{E}} / \Omega \tag{5}$$

式中, Ω为植被冠层聚集度系数, 与地表覆盖类型、季节和太阳高度角等有关。由于没有聚集度系数空间分布资料, 在本研究中仅考虑了该参数随植被类型的变化(表 1) (Tang 等, 2007)。

3.2 使用的数据

反演 LAI 所需的红光波段反射率、近红外波段反射率、短波红外波段反射率、太阳天顶角、传感

表 1 不同植被类型的聚集度系数

植被类型	聚集度系数
常绿阔叶林	0.63
落叶阔叶林	0.70
常绿针叶林	0.62
落叶针叶林	0.68
混交林	0.69
高郁闭度灌木	0.71
稀疏灌木	0.71
木质热带稀树草原	0.72
热带稀树草原	0.70
草地	0.74
农作物	0.73

器天顶角、太阳和卫星相对方位角数据从 MODIS 产品数据库中下载; 全球地表覆盖分类数据从相应的网站下载; 验证 LAI 反演精度的 30 m TM LAI 数据由根据 LAI 观测数据和 TM 光谱数据建立的经验模型生成。

3.2.1 LAI 观测和 30 m TM LAI 图像的生成

于 2008 年 7 月 24—27 日, 在晴朗天气条件下, 选择研究区内有代表性的 47 个森林样地, 使用 TRAC 进行 LAI 的观测, 每个样地的大小为 30m×30m, 与 TM 影像的像元大小一致, 观测时间为 9:30—16:30。观测按照 TRAC 的使用规范进行, 同时使用 GPS 记录观测点的经、纬度和海拔高度。

为了生成研究区的 30 m TM LAI 图像用于评价 LAI 的反演精度, 本研究一共使用了 3 景 TM 影像, 成像时间分别为 2008-07-26(122/41, 122/42) 及 2008-05-16 (121/41), 其中, 2008-07-26 的 122/41 影像覆盖了研究区的大部。在拼接前对各景图像进行几何精校正和大气校正处理。几何精校正采用 ENVI 软件进行, 以获取的江西省森林资源遥感调查影像为参考, 收集特征明显的控制点, 对整幅图像进行校正, 校正的总体误差(RMSE)控制在 1 个像元以内, 采用投影方式为 UTM/WGS 84。经过几何精校正后, 采用 6S 模型(Vermote 等, 1997)对图像进行大气校正, 生成反射率图像。运行 6S 模型时, 大气模式设置为中纬度夏季模式, 气溶胶类型设置为大陆型, 大气的能见度设置为 30 km。对经过几何校正和大气校正的 3 景影像进行拼接, 利用吉安市的行政边界对拼接的图像裁剪, 得到研究区的反射率影像。

根据反射率数据生成了多种植被指数, 计算它们与观测的 LAI 之间的相关系数, 发现经过指数形式变换后, NDVI 与观测的 LAI 之间的相关性最高 (R^2=0.68, RMSE=0.25, N=47) (Li 等, 2009), 利用该模型得到的 47 个样点 LAI 的平均值为 2.77, 而观测数据的平均值为 2.88。所以, 采用由 NDVI 建立的 LAI 经验模型($LAI=0.0284e^{7.7357NDVI}$)生成研究区的 30 m 的 LAI 图像, 再对该图像采样到 1km 和 4 km, 用于验证反演的 LAI 精度。图 1 是生成的 30 m 分辨率的 TM LAI 分布图, 由于实测 LAI 数据中没有农作物样本, 所以仅计算了森林的 LAI。从图 1 看出, 研究区内森林的 LAI 空间变化比较明显, 其中在东部和西北部, LAI 为 3—5, 在西南部地区, LAI 较高, 普遍在 6 以上。

3.2.2 MODIS 反射率数据

反演 LAI 使用的反射率数据为 8d 合成的 MODIS 500m MOD09A1 产品, 生成时间为 2008-07-28, 投影方式为 Sinusoidal, 为了与其他数据进行匹配, 将投影转换为 UTM/WGS 84, 并采样到 1km。该产品由 7 个反射率数据波段、数据质量描述波段和 3 个角度信息波段组成。由于模型仅需要输入红光、近红外和短波红外 3 个波段的反射率、质量信息和 3 个角度信息数据, 从 MOD09A1 产品中剔除多余的波段组成一个新的数据文件并用吉安市行政边界数据裁剪出研究区的数据。

3.2.3 地表覆盖分类数据

研究采用了 6 种地表覆盖分类数据, 包括下载的 5 种全球地表覆盖分类数据和江西省气象局提供的 1996 年利用 TM 数据生成的 30 m 分辨率的江西省森林资源遥感调查数据, 该数据将地表覆盖分为阔叶林、针叶林、针阔混交林、竹林、疏林、灌木林、无立木林地、荒地、农田、水体、山地阴影、

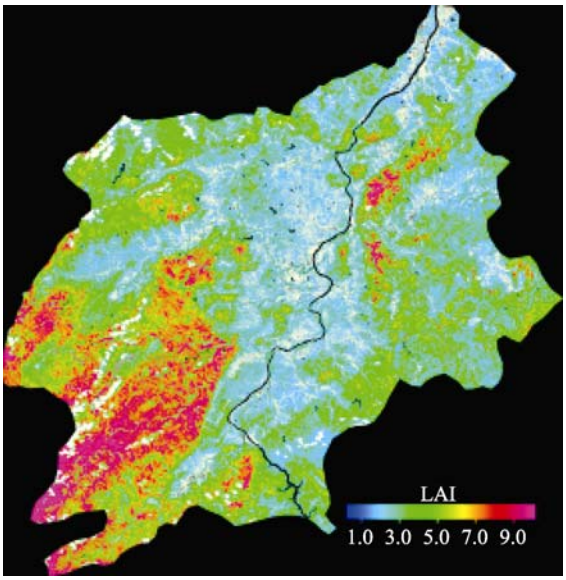

图 1 经验模型生成的研究区 30m TM LAI 分布图

城镇居民点、草地和鄱阳湖草洲等 14 类。为方便起见, 下文中简称该数据为 TM 地表覆盖分类数据, 采用面积最高比例法(采样后的地表覆盖类型设为面积比例最高的地表覆盖类型)将该数据采样成 1 km 分辨率的数据。5 种全球地表覆盖分类数据分别为马里兰大学利用 1992—1993 年的 AVHRR 数据, 采用基于时间矩阵的监督分类方法生成的全球地表覆盖分类数据(简称为 UMD 全球地表覆盖分类数据), 该数据包含的全球地表覆盖类型为 14 类; 美国地质调查局(USGS)、内布拉斯加林肯大学(UNL)和欧共体的联合研究中心合作利用 1992—1993 年的 AVHRR 数据, 采用非监督分类方法生成的全球地表覆盖分类数据 (简称为 USGS 全球地表覆盖分类数据), 该数据将全球地表覆盖分为 24 类; 波士顿大学利用 2000—2001 年的 MODIS 数据和神经元网络与决策树算法生成的全球地表覆盖分类数据(简称为 MODIS 全球地表覆盖分类数据), 该数据将全球地表覆盖分成 17 类, 包括 11 个自然植被类、3 个人工地类、雪和冰、永久裸地或稀疏植被和水体。以上这 3 种数据的空间分辨率均为 1km, 采用的是国际地圈生物圈计划(IGBP)的分类体系。第 4 种全球地表覆盖数据是欧洲联合研究中心空间研究所利用 1999 年 11 月至 2000 年 12 月 SPOT/VEGETATION 日序列的地表反射率和 NDVI 生成的 GLC2000 全球地表覆盖数据, 该数据按照联合国粮农组织(FAO)地表覆盖分类体系(LCCS), 采用自底向上的分类方法将全球土地覆盖分成 22 类。第 5 种全球地表覆盖数据是欧洲航天局联合其他国际机构组织共同建立的全球 300 m 分辨率的地表覆盖分类数据 GLOBCOVER, 生成该数据使用的是 2004 年 12 月至 2006 年 6 月共 20 个月的 300 m 分辨率的 ENVISAT/MERIS 系列资料, 对每 2 个月的资料进行一次合成共生成 10 次用于分类的数据, 按照 LCCS 分类体系, 采用计算机自动分类和区域调整分类方法将土地覆盖分成 22 类, 为了与其他数据的空间分辨率保持一致, 对该数据也采用面积最高比例法采样到 1km。

上述 6 种地表覆盖分类数据使用的分类体系和分类代码存在着差异, 本文使用的 LAI 反演模型需要输入按照 IGBP 分类体系和 MODIS 地表覆盖分类代码生成的地表覆盖数据。所以, 对 USGS、UMD、GLC2000、GLOBCOVER 和 TM 等 5 种地表覆盖分类数据进行了分类转换, 以满足 LAI 反演模型的需要。表 2 给出了不同地表覆盖分类数据的转换关系。

3.3 地表覆盖分类数据对 LAI 反演精度的影响评价

将反演的 LAI 与 TM 数据生成的 LAI 进行比较, 评价地表覆盖分类数据对 LAI 反演精度的影响, 由于研究区存在大量的森林与非森林的混合像元, 基于每个 30m 的像元都是纯像元的假设, 分别统计每个 1km 和 4km 像元内森林的比例, 仅对森林面积比例大于 50%的 1km 和 4km 像元进行 LAI 反演的精

表 2 5 种不同地表覆盖分类数据的分类体系与 IGBP/MODIS 分类体系的转换关系

IGBP/MODIS 类型	USGS	UMD	GLOBCOVER	GLC2000	TM
1 常绿针叶林	14	1	70	4, 10	2, 4, 12
2 常绿阔叶林	13	2	40, 160, 170	1, 7, 8	1
3 落叶针叶林	12	3	90	5	-
4 落叶阔叶林	11	4	50, 60	2, 3	-
5 混交林	15	5	100, 110, 120	6, 9	3
6 高郁闭度灌木	8	8	130	11, 12	6
7 稀疏灌木	9	9	150	14	-
8 木质热带稀树草原	21	6	-	-	5
9 热带稀树草原	10, 20, 22	7	-	-	7
10 草地	7	10	140	13	8
11 永久湿地	17, 18	-	180	15	14
12 农作物	2, 3, 4	11	11, 14	16	10
13 城镇建设用地	1	13	190	22	13
14 农作物/自然植被混合	5, 6	-	20, 30	17, 18	-
15 雪和冰或永久裸地	23, 24	12	220	21	-
16 稀疏植被/裸地	19	-	200	19	9
17 水体	16	0	210	20	11

度评价。使用的评价指标包括反演的 LAI 与 TM LAI 之间的相关系数, 反演的 LAI 与 TM LAI 比较的均方根误差(RMSE)和平均值的相对差。

4 结果与分析

4.1 地表覆盖分类数据一致性分析

表 3 给出了根据不同地表覆盖分类数据统计的研究区内各地表覆盖类型的面积比例, 存在着很大的差别。在 USGS 和 UMD 地表覆盖分类数据中, 森林占的面积很少, 不到 10%, 这与本研究区的实况不符, 吉安市的森林资源非常丰富, 据统计该市的森林覆盖率高达 65.5%。在 MODIS、GLOBCOVER、GLC2000 和 TM 4 种地表覆盖分类数据中, 森林占的比例在 50%以上, 与当地实际较为一致, 但这 4 种地表覆盖分类数据在森林类型上存在着很大的差别, GLOBCOVER 和 TM 地表覆盖分类数据中针叶林所占比重比较大, 分别为 41.77%和 37.64%, 与实际吻合; MODIS 地表覆盖分类数据中混交林比例最高为 40.66%; 而在 GLC2000 数据中落叶阔叶林的比例高达 62.97%。热带稀树草原类型在 GLOBCOVER 和 GLC2000 数据中不存在, 但在 USGS 和 UMD 地表覆盖分类数据中的比例分别高达 41.09%和 48.17%。GLC2000 与其他 5 种地表覆盖分类数据在水体、农作物和城镇等类型所占比例差别较大, 农作物在本研究区占有相当的比例, GLC2000 数据中农作物所占比例为 0, 而其他 5 种地表覆盖分类数据中农作物的比例均超过了 15%。吉安市地处中纬度亚热带, 是一个没有雪和冰覆盖的地区, 但在 GLC2000 地表覆盖分类数据中, 冰与雪的比例却达到了 14.23%。这些地表覆盖分类数据的差异有可能是分类体系和分类差异所造成, 也可能是由于数据生成的时间不同所引起。

4.2 反演的 LAI 分布特征

由 6 种地表覆盖分类数据和 MODIS 反射率及角度数据反演的吉安市 1 km LAI 存在着较大的差异(图 2)。利用 MODIS、GLOBCOVER 和 TM 地表覆盖分类数据反演的 LAI 在空间分布上较为一致, 空间变化明显, 表现出西部森林 LAI 高于东部森林 LAI 的特征(图 2(d)、(e)和(f)), 但由 GLOBCOVER 和 TM 地表覆盖分类数据反演的高 LAI 值(>7)的比例高于利用 MODIS 地表覆盖分类数据反演的结果。利用这 3 种地表覆盖分类数据反演的 LAI 的空间分布特征与 TM 数据生成的 30 m LAI 的空间分布特征具有较高的相似性, 但在西北部, 反演的 LAI 明显高于 TM 数据生成的 30 m LAI。利用 UMD 和 USGS 地表覆盖分类数据反演的 LAI 空间变化不明显(图 2(b)、(c)), 在西部反演的 LAI 明显低于 TM LAI, 整个研究区内森林的 LAI 主要处于 3—5, 7 以上的部分很少, 特别是 USGS 数据反演的 LAI 几乎

表 3 不同地表覆盖分类数据中各地表覆盖类型所占面积比例

/%

地表覆盖类型	USGS	UMD	GLOBCOVER	GLC2000	MODIS	TM
常绿针叶林	4.32	9.04	41.77	0	5.56	37.64
常绿阔叶林	0	0.24	13.60	0	3.12	1.28
落叶针叶林	0	0	0	17.41	0.02	0
落叶阔叶林	1.79	0.08	0.03	62.97	1.46	0
混交林	0.22	0.18	0.63	0.23	40.66	10.35
高郁闭度灌木	0.18	0.06	9.88	0	0.36	4.27
稀疏灌木	0	0.03	0	0.65	0.60	0
木质热带稀树草原	0	17.93	0	0	25.02	0.47
热带稀树草原	41.09	30.24	0	0	0.65	3.77
草地	0.19	25.38	0.03	0	1.97	0.66
永久湿地	0.01	0	0	4.49	1.71	0
农作物	30.63	15.71	30.31	0	16.43	36.87
城镇建设用地	0.03	0.03	0.21	0	0.20	1.67
农作物/自然植被混合	20.52	0	2.49	0	1.89	0
雪和冰或永久裸地	0	0	0	14.23	0	0
稀疏植被/裸地	0	0	0	0	0.03	0.14
水体	1.02	1.09	1.05	0	0.32	2.88

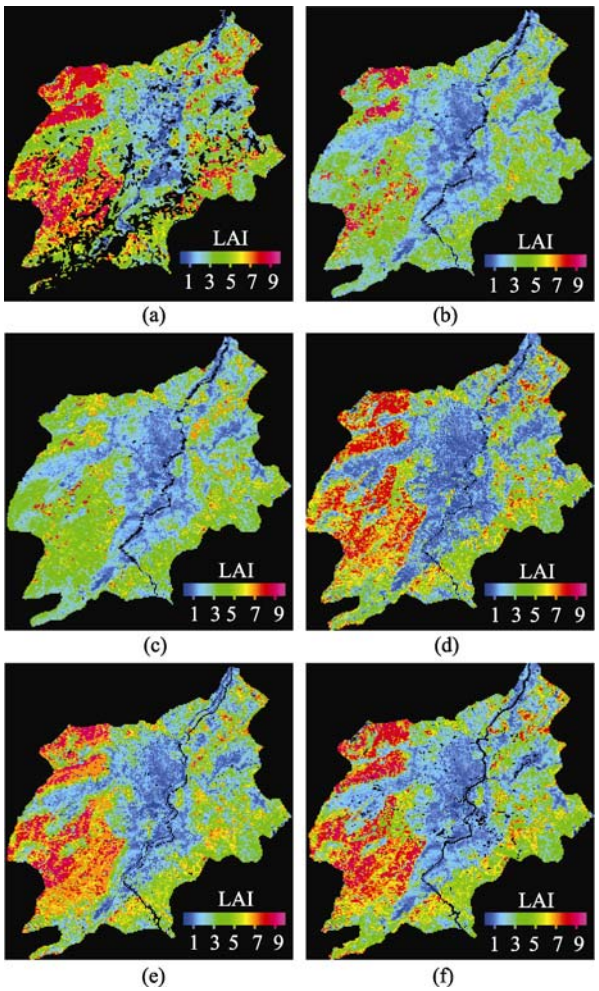

图 2 利用 GLC2000(a)、UMD(b)、USGS(c)、MODIS(d)、GLOBCOVER(e)和 TM(f)地表覆盖分类数据反演的 1km LAI 分布图

小于 7 (图 2(c))。由于 GLC2000 地表覆盖分类数据与其他地表覆盖分类数据的差别较大, 据其反演的 LAI (图 2(a))与利用其他地表覆盖分类数据反演的 LAI 在东部差异明显, 在该地表数据中, 部分森林和农田被错分为雪和冰, 其反演的 LAI 为 0(图 2(a)中的黑色区域)。总体而言, 利用 6 种地表覆盖分类数据反演的 LAI 的一致性在中部和东部好于西部。

4.3 地表覆盖分类数据对 LAI 反演精度的影响

表 4 给出了利用不同的地表覆盖分类数据反演 1km 森林 LAI 与 TM LAI 重采样数据比较的统计结果。在 6 种地表覆盖分类数据中, TM 地表覆盖分类数据参与反演 LAI 的结果最好, 据其反演的 LAI 与 TM LAI 之间的相关性最高(R^2=0.44); 其次为 GLOBCOVER 地表覆盖分类数据, 利用该数据反演的 LAI 与 TM LAI 相关的 R^2 为 0.40; UMD 和 GLC2000 地表数据会导致反演的 LAI 存在大的误差, 据其反演的 LAI 与 TM LAI 之间相关的 R^2 分别为 0.24 和 0.15。反演的 LAI 与 TM LAI 比较的 RMSE 最大为 2.7(利用 GLC2000 的反演结果), 最小为 1.8(利用 TM 分类数据反演的结果)。利用 GLC2000、GLOBCOVER 和 TM 分类数据反演的研究区内森林 LAI 的平均值比 TM LAI 的平均值偏高 3.4%、5.1%和 2.4%, 利用其他 3 种地表覆盖分类数据反演的 LAI 的平均值偏低, 其中 UMD 和 USGS 数据导致反演的 LAI 平均值偏低 19.8%和 18.8%。

为了减小不同遥感图像配准误差对 LAI 反演精度评价结果的影响, 在 4km 尺度上将反演生成的 LAI 与 30m TM LAI 的采样数据进行比较。利用 6 种地表覆盖分类数据反演的 LAI 与 TM LAI 数据一致性在 4 km 尺度上明显上升, 利用 TM 地表覆盖分类数据反演的 LAI 与 TM LAI 相关 R^2 最高, 达到了 0.57, GLC2000 反演的 LAI 与 TM LAI 相关 R^2 最低, 为 0.23。与 1 km 尺度的比较结果一样, 利用 TM、

表 4 利用 6 种地表覆盖分类数据反演的 LAI 与 TM LAI 比较的统计结果

不同地表覆盖数据反演的 LAI	1 km				4 km			
	R^2	RMSE*	平均值**	RE***	R^2	RMSE*	平均值**	RE***
GLC2000	0.15	2.7	4.2	3.4%	0.23	2.1	3.96	–1.0%
UMD	0.24	2.1	3.2	–19.8%	0.34	1.8	3.1	–21.8%
USGS	0.30	2.0	3.3	–18.8%	0.40	1.6	3.2	–20.5%
MODIS	0.38	1.9	3.9	–4.1%	0.51	1.5	3.8	–5.7%
GLOBACOVER	0.40	1.9	4.3	5.1%	0.54	1.4	4.1	3.1%
TM	0.44	1.8	4.2	2.4%	0.57	1.3	4.0	1.8%

* $\mathrm{RMSE}=\sqrt{1/N\sum_{i=1}^{N}(\mathrm{LAI}_{\mathrm{inv}}(i)-\mathrm{LAI}_{\mathrm{TM}}(i))^2}$, N 为森林类型的像元数, $\mathrm{LAI}_{\mathrm{inv}}$ 和 $\mathrm{LAI}_{\mathrm{TM}}$ 分别为反演的 LAI 和由 30 m TM LAI 采样生成的 LAI;

**研究区内反演的所有森林像元 LAI 的平均值 $=\frac{1}{N}\sum_{i=1}^{N}\mathrm{LAI}_{\mathrm{inv}}(i)$ 。

***RE 为平均值相对差, $\mathrm{RE}=(\overline{\mathrm{LAI}_{\mathrm{inv}}}-\overline{\mathrm{LAI}_{\mathrm{TM}}})/\overline{\mathrm{LAI}_{\mathrm{TM}}}\times100\%$, $\overline{\mathrm{LAI}_{\mathrm{inv}}}$ 是反演的 LAI 的平均值, $\overline{\mathrm{LAI}_{\mathrm{TM}}}$ 是由 30 m TM LAI 采样生成的 LAI 的平均值。

GLOBCOVER 和 MODIS 地表覆盖分类数据反演的 LAI 精度优于利用其他 3 种地表覆盖分类数据反演的 LAI 精度。与 1km 尺度的比较结果相比, 反演 LAI 的 RMSE 有所下降, 最小为 1.3(利用 TM 分类数据的反演结果), 最大为 2.1(利用 GLC2000 的反演结果), 但是平均值的相对差变化不明显(表 4)。

4.4 LAI 反演结果对模型参数的敏感性分析

与地表覆盖类型有关的聚集度系数(Ω)、短波红外反射率的最大值($\rho_{SWIRmax}$) 和最小值($\rho_{SWIRmin}$)是利用式(4)和式(5)反演 LAI 的关键参数, 为了评价这些参数取值对 LAI 反演结果的影响, 进行了 LAI 反演结果对这些参数的敏感性分析试验, 即分别将这些参数值增加和减小 10%进行 LAI 的反演, 将反演结果与 TM LAI 进行比较, 确定参数值的变化导致的 LAI 反演结果变化程度。表 5 给出了在 4 km 尺度, 利用不同的地表覆盖分类数据反演的 LAI 与 TM LAI 比较的统计结果。如Ω增大 10%, 利用所有的地表覆盖分类数据反演的 LAI 的平均值比 TM LAI 的平均值偏低, 如Ω减小 10%, 利用 UMD 和 USGS 地表覆盖分类数据反演的 LAI 与 TM LAI 之间的一致性得到增强。由方程(4)可以发现, 改变$\rho_{SWIRmax}$ 和$\rho_{SWIRmin}$ 将导致 L_E 反演结果的改变, 从而影响 LAI 的反演结果, $\rho_{SWIRmax}$和$\rho_{SWIRmin}$的增大会引起反演的 LAI 增大; 反之, $\rho_{SWIRmax}$和$\rho_{SWIRmin}$的减小会引起反演的 LAI 减小, 但是 LAI 对$\rho_{SWIRmax}$和$\rho_{SWIRmin}$的响应是非线性的。LAI 反演结果对Ω的敏感性大于对$\rho_{SWIRmax}$和$\rho_{SWIRmin}$的敏感性。

表 5 4 km LAI 反演结果对模型参数的敏感性分析结果

地表覆盖分类数据	1.1Ω			0.9Ω			$1.1\rho_{SWIRmax}$			$0.9\rho_{SWIRmax}$			$1.1\rho_{SWIRmin}$			$0.9\rho_{SWIRmin}$		
	R^2	RMSE	RE*	R^2	RMSE	RE	R^2	RMSE	RE	R^2	RMSE	RE	R^2	RMSE	RE	R^2	RMSE	RE
GLC2000	0.23	2.0	–8.3	0.23	2.1	7.2	0.24	2.1	6.4	0.22	2.1	–10.4	0.23	2.0	0.6	0.23	2.0	–2.3
UMD	0.32	1.9	–27.9	0.36	1.6	–14.6	0.34	1.8	–21.1	0.34	1.8	–22.7	0.34	1.7	–21.6	0.34	1.8	–22.0
USGS	0.38	1.8	–26.6	0.42	1.5	–13.1	0.39	1.6	–19.7	0.41	1.6	–21.3	0.40	1.6	–20.3	0.40	1.6	–20.6
MODIS	0.50	1.5	–12.5	0.53	1.4	2.0	0.53	1.4	–1.4	0.49	1.5	–11.0	0.51	1.5	-4.9	0.51	1.5	–6.4
GLOBACOVER	0.54	1.4	–4.1	0.54	1.5	11.5	0.55	1.5	7.1	0.53	1.4	–1.8	0.54	1.4	4.1	0.54	1.4	2.3
TM	0.57	1.4	–0.2	0.57	1.3	4.5	0.59	1.4	6.3	0.54	1.3	–3.6	0.57	1.4	2.9	0.57	1.3	0.9

*RE 为平均值相对差, 计算方法同表 4。

5 结论与讨论

本文利用不同的地表覆盖分类数据与 MODIS 反射率数据产品结合, 反演研究区的 LAI, 以 TM 数据生成的 LAI 作为标准, 评价地表覆盖分类数据质量对区域尺度 LAI 反演精度的影响。通过研究, 得到以下结论:

(1) 6 种地表覆盖分类数据(MODIS、USGS、GLOBCOVER、UMD、GLC2000、TM)在分类结果上有比较大的差别, 这种差别主要由于分类方法、使用的数据源以及采用的分类体系不同导致。这些差别导致利用不同的地表覆盖分类数据反演的研究区内 LAI 的平均值相差达 20%以上。因此, 要提高区域 LAI 反演的精度, 需要可靠的地表覆盖分类数据的支持。

(2) 在 6 种地表覆盖分类数据中, 利用 TM 地表覆盖分类数据反演的 LAI 的精度最高, 在 1km 和 4km 尺度上反演的 LAI 与 TM LAI 相关的 R^2 分别为 0.44 和 0.57, 而平均值的相对误差为 2.4%和 1.8%。在 5 种全球地表覆盖分类数据中, GLOBCOVER 和 MODIS 具有较好的 LAI 反演结果, 可以用于研究区内 LAI 的反演。GLC2000 和 UMD 地表覆盖分类数据会导致研究区内 LAI 反演结果出现较大的误差。

(3) 敏感性分析表明, 聚集度系数(Ω)对 LAI 的反演结果有显著的影响($LAI=LAI_E/\Omega$),本文仅考虑了该参数随植被类型的变化, 未考虑其还随森林的演替阶段和季节变化, 增加了 LAI 反演结果的不确定性。如能利用多角度遥感资料提取聚集度系数, 将可以提高 LAI 反演的精度。

反演的 LAI 的精度是根据 TM30m LAI 数据进行评价的, 该数据由利用观测资料建立的 LAI 经验估算模型生成。毫无疑问, TM 30 m LAI 数据存在着一定的误差, 会对评价结果产生一定的影响。不同的 LAI 反演模型对地表覆盖分类数据的敏感性存在着差异, 本文仅利用基于 4 尺度几何光学模型的 LAI 反演模型研究地表覆盖分类数据对 LAI 反演结果的影响, 未使用更多的反演模型进行研究, 这是本文的不足之处, 有待进一步改进。此外, 地表覆盖分类数据仅是影响 LAI 反演结果的一个重要方面, 对于森林 LAI 反演而言, 地形效应和背景反射干扰

等因子也会对 LAI 的反演结果产生显著影响, 在本研究中未考虑这些因子的作用, 这是导致反演的 LAI 与 TM LAI 存在着一定差异的一个原因。在利用 MODIS 光谱数据反演 LAI 时, 如何利用 MISR 等多角度遥感数据提取背景反射率和对光谱数据进行地形订正, 是今后应该努力的方向。

REFERENCES

Bartholomé E and Belward S. 2005. GLC2000: a new approach to global land covers mapping from earth observation data. *International Journal of Remote Sensing*, **26**(9): 1959—1977

Brown L, Chen J M, Leblanc S G and Cihlar J. 2000. A shortwave infrared modification to the simple ratio for LAI retrieval in boreal forests: an image and model analysis. *Remote Sensing of Environment*, **71**: 16—25

Chen J M and Cihlar J. 1996. Retrieving leaf area index of boreal conifer forests using Landsat TM images. *Remote Sensing of Environment*, **55**: 153—162

Defourny P, Vancutsem C, Bicheron P, Nino F, Schouten L and Leroy M. 2006. Globcover: a 300 m global land cover product for 2005 using ENVISAT MERIS time series. Proceedings of ISPRS Commission VII Symposium: Remote Sensing from Pixels to Processes. Enschede, The Netherlands

Deng F, Chen J M, Plummer S, Chen M Z and Pisek J. 2006. Algorithm for global leaf area index retrieval using satellite imagery. *IEEE Transactions on Geoscience and Remote Sensing of Environment*, **44**(8): 2219—2229

Fang X Q and Zhang W C. 2003. The application of remotely sensed data to the estimation of the leaf area index. *Remote Sensing for Land & Resources*, (3): 58—62

Friedl M A, McIver D K, Hodges J C F, Zhang X Y, Muchoney D, Strahler A H, Woodcock C E, Gopal S, Schneider A, Cooper A, Baccini A, Gao F and Schaaf C. 2002. Global land cover mapping from MODIS: algorithms and early results. *Remote Sensing of Environment*, **83**: 287—302

Garrigues S, Lacaze R, Baret F, Morisette J T, Weiss M, Nickeson J E, Fernandes R, Plummer S, Shabanov N V, Myneni R B, Knyazikhin Y and Yang W. 2008. Validation and intercomparison of global Leaf Area Index products derived from remote sensing data. *Journal of Geophysical Research*, **113**, G02028, doi:10.1029/2007JG000635

Hansen M C, DeFries R S, Townshend J R G and Sohlberg R. 2000. Global land cover classification at 1km spatial resolution using a classification tree approach. *International Journal of Remote Sensing*, **21**(6/7): 1331—1364

Herold M, Mayaux P, Woodcock C E, Baccini A and Schmullius C. 2008. Some challenges in global land cover mapping: An assessment of agreement and accuracy in existing 1 km datasets. *Remote Sensing of Environment*, **112**: 2538—2556

Li X F, Ju W M, Zhou Y L and Chen S. 2009. Retrieving leaf area index of forests in red soil hilly region using remote sensing data. Proceedings of the Second International Conference on Earth Observation for Global Changes.

Liu R, Chen J M, Liu J, Deng F and Sun R. 2007. Application of a new leaf area index algorithm to China's landmass using MODIS data for carbon cycle research. *Journal of Environmental Management*, **85**: 649—658

Loveland T R, Reed B C, Brown J F, Ohlen D O, Zhu Z Yang L and Merchant J W. 2000. Developments of a global land cover characteristics database and IGBP DISCover from 1-km AVHRR Data. *International Journal of Remote Sensing*, **21** (6/7): 1303—1330

Pisek J, Chen J M and Deng F. 2007. Assessment of a global leaf area index product from SPOT-4 vegetation data over selected sites in Canada. *Canadian Journal of Remote Sensing*, **33**(4): 341—358

Quaife T, Quegan S, Disney M, Lewis P, Lomass M and Woodward F I. 2008. Impact of land cover uncertainties on estimates of biospheric carbon fluxes. *Global Biogeochemical Cycles*, **22**, GB4016, doi:10.1029/2007GB003097

Sellers P J, Dickinson R E, Randall D A, Betts A K, Hall F G, Berry J A, Collatz G J, Denning A S, Mooney H A, Nobre C A, Sato N, Field C B and Henderson-sellers A. 1997. Modeling the Exchanges of energy, water, and carbon between continents and the atmosphere. *Science*, **275**: 502—509

Tang S, Chen J M, Zhu X, Li X Chen M, Sun R, Zhou Y, Deng F and Xie D. 2007. LAI inversion algorithm based on directional reflectance kernels. *Journal of Environmental Management*, **85**: 638—648

Vermote E F, Tanre D, Deuze' J L, Herman M and Morcrette J J. 1997. Second simulation of the satellite signal in the solar spectrum, 6S: an overview. *IEEE Transactions on Geoscience and Remote Sensing of Environment*, **35**(3): 675—686

附中文参考文献

方秀琴, 张万昌. 2003. 叶面积指数的遥感定量方法综述. 国土资源遥感, (3): 58—62